

# RSC Advances



This is an *Accepted Manuscript*, which has been through the Royal Society of Chemistry peer review process and has been accepted for publication.

*Accepted Manuscripts* are published online shortly after acceptance, before technical editing, formatting and proof reading. Using this free service, authors can make their results available to the community, in citable form, before we publish the edited article. This *Accepted Manuscript* will be replaced by the edited, formatted and paginated article as soon as this is available.

You can find more information about *Accepted Manuscripts* in the [Information for Authors](#).

Please note that technical editing may introduce minor changes to the text and/or graphics, which may alter content. The journal's standard [Terms & Conditions](#) and the [Ethical guidelines](#) still apply. In no event shall the Royal Society of Chemistry be held responsible for any errors or omissions in this *Accepted Manuscript* or any consequences arising from the use of any information it contains.

Cite this: DOI: 10.1039/c0xx00000x

www.rsc.org/xxxxxx

ARTICLE TYPE

# Development of New Graphene Oxide Incorporated Tricomponent Scaffolds with Polysaccharides and Hydroxyapatite and Study of their Osteoconductivity on MG-63 Cell Line for Bone Tissue Engineering

R. Rajesh, Y. Dominic Ravichandran\*

5 Received (in XXX, XXX) Xth XXXXXXXXXX 20XX, Accepted Xth XXXXXXXXXX 20XX

DOI: 10.1039/b000000x

## Abstract

Regenerative medicine witness a paradigm shift from synthetic implants and tissue grafts to a tissue engineering approach that incorporates biodegradable, bioceramic composite scaffolds with biological cells. A combination of carbon nanomaterials and hydroxyapatite (HAP) with polysaccharides hold a great potential in bone tissue engineering. In the present study, new porous tricomponent scaffolds, graphene oxide (GO)-gellan-HAP, GO-alginate-HAP and GO-amylopectin-HAP were prepared by freeze drying method. The ionic interactions between the individual components in the formation of the composites were confirmed by FTIR and XRD. The porous morphology of scaffolds was confirmed by FE-SEM images. Osteoconductivity and biocompatibility of scaffolds on MG 63 cell line were confirmed by *in vitro* MTT assay. The increased mineralization could be visualized by alkaline phosphatase (ALP) activity. Among the scaffolds, the GO-amylopectin-HAP exhibited higher biocompatibility, mineralization and cell attachment. The compressive strength values were determined and found to be  $466.8 \pm 19$  for GO-gellan-HAP,  $171 \pm 17$  for GO-alginate-HAP and  $161 \pm 4$  for GO-amylopectin-HAP scaffolds. The higher biocompatibility, mineralization and cell attachment and lower compressive strength for GO-amylopectin-HAP was attributed to higher pore size and porosity. These results indicated that the prepared tricomponent scaffolds could be used as promising biomaterials in tissue engineering.

## Introduction

Tissue engineering for bone is a multifarious and dynamic process that initiates with migration and recruitment of osteoprogenitor cells followed by their proliferation, differentiation, matrix formation along with remodelling of the bone.<sup>1</sup> Recently, different biomaterials are investigated in the field of tissue engineering to overwhelm the hurdles which are essential for it to be successful in clinical applications.<sup>2</sup> The essential properties required for an ideal scaffold in tissue engineering include osteoinduction, osteoconductivity, mechanical strength, porosity, mineralization, biodegradability and bioresorbability. An ideal 3D scaffold facilitates cells to undergo differentiation, proliferation and the ability to transfer cells and bioactive materials to defective sites for the new tissue formation. Further, it should be stable for a specific period of time to facilitate the body to get healed or to regain the ability to get healed. Then, the scaffold should biodegrade or become non-

functional. Hence, biodegradable natural polysaccharides that are similar to biological macromolecules or that which can mimic natural extracellular matrix (ECM) are chosen to develop scaffolds.<sup>3-9</sup> Some of the biodegradable natural polysaccharides reported for tissue engineering applications are alginic acid,<sup>10</sup> amylopectin, chitin, chitosan, chondritine sulfate,<sup>11</sup> gellan gum,<sup>12</sup> hyaluronic acid<sup>13</sup> and xanthan gum.<sup>14</sup>

HAP is an important bioceramic in bone tissue engineering because of its similarity to the inorganic minerals present in the natural bone.<sup>15,16</sup> It is used in several biomedical applications including drug delivery,<sup>17</sup> orthopedics, dentistry, maxillofacial,<sup>18</sup> bone and wound tissue engineering<sup>19</sup> due to its biocompatibility, bioactivity and osteoconductivity.<sup>20</sup> The carbonated HAP isolated from natural sources has several advantages like higher biocompatibility and bioresorption than synthesized HAP.<sup>21,22</sup> Hence, natural HAP isolated from chicken bones<sup>23</sup> are used in this study. The healing rate depends on the location of bone tissue in the human body. In order to mimic the role of bone, polymer-HAP composite should possess mechanical strength, resorption and biodegradation.<sup>2</sup>

The carbon based nano fillers such as carbon black, carbon nanotubes (CNTs), expanded graphite, graphene (GP) and carbon nanofiber were used as an excellent filler material in order to improve mechanical strength. CNTs are effective filler material

40 Organic Chemistry Division, School of Advanced Sciences, VIT University, Vellore-632014, Tamilnadu, India.

\* Corresponding author: Fax: +91-416-2243092, +91-416-2245766 E-mail address: [ydominic64@yahoo.co.in](mailto:ydominic64@yahoo.co.in)

† Electronic Supplementary Information (ESI) available: [details of any supplementary information available should be included here]. See DOI: 10.1039/b000000x/

but its higher production cost created a need for the low cost GP as an alternative.<sup>24,25</sup> The hydrophobic nature of GP tends to form irreversible agglomeration in aqueous solution due to the strong  $\pi$ - $\pi$  stacking interactions. Hence, the oxidised form of GP, GO with the presence of hydroxyl, carboxyl and epoxy groups emerge as a replacement due to greater interaction with proteins through covalent, electrostatic and hydrogen bonding. Further, it also improves the interfacial interaction with hydrophilic polymers.<sup>26-28</sup> Previous studies revealed that the incorporation of GO in scaffolds not only enhanced the mechanical properties but also activate the functions of osteoblast culture.<sup>29</sup> Hence, GO has created much attention in biomedical applications including bioassays, biosensors, bio-imaging, drug delivery and tissue engineering.<sup>24,27,30</sup>

The preparation of tricomponent scaffolds has gained increased attention in recent times due to the reason that it can mimic the natural bone. Since the natural bone is composed of organic and inorganic materials, bioresorbable polysaccharides (gellan, alginate and amylopectin) are used as organic material and bioactive carbonated HAP as inorganic mineral in this study. Further, GO has been included as effective filler material for increasing the mechanical strength. The combination of polysaccharides with HAP and GO showed improved osteoconductivity with increased mechanical strength. Moreover, osteoconductive biomaterials act as a passive site for cellular adhesion, proliferation and differentiation.<sup>31</sup> Ideal scaffolds should be porous in order to allow cell to in growth, migrate and permit the efficient transport of nutrients along with the removal of cellular waste product. Further, porosity can increase the biodegradation of the implant material by increasing the surface area in contact with body fluids. This may enhance osteoconductivity but decreases the mechanical strength. The mechanical strength of the scaffolds are improved by the addition of GO. Hence, freezing and lyophilisation method was used to prepare porous scaffolds which has the advantages of simplicity in procedure and minimal equipments.<sup>32-37</sup> There are many tricomponent scaffolds like multi walled carbon nanotube (MWCNT)-chitosan-HAP,<sup>21</sup> MWCNT-gelatin-HAP,<sup>38</sup> GO-chitosan-HAP<sup>18</sup> and GO-hyaluronic acid-HAP<sup>39</sup> which have already been reported. To best of our knowledge, we report the preparation, characterization, compressive strength, *in vitro* osteoconductivity and ALP activity of new tricomponent scaffolds of GO-alginate-HAP, GO-amylopectin-HAP and GO-gellan gum-HAP on MG-63 cell line for the first time. The hydrophilic nature possessed by the components present in the scaffolds enhances the cell adhesion and proliferation. All the tricomponent scaffolds showed better cell proliferation, differentiation and compressive strength based on their porosity.

## Result and Discussion

### Thermal stability

The thermo gravimetric analysis of the scaffold materials was shown in Fig. 1. The first weight loss was observed between 30 °C to 180 °C in the scaffold materials due to the evaporation of absorbed water molecules.<sup>22</sup> Further, the major weight loss was between 214 °C to 580 °C in GO-gellan-HAP, 209 °C to 568 °C in GO-alginate-HAP and 186 °C to 586 °C in GO-amylopectin-

HAP was attributed to the thermal decomposition of gellan, alginate and amylopectin into carbonaceous material and combustion of GO. The negligible amount of weight loss observed above 600 °C indicated the thermal stability of HAP.<sup>18,40-42</sup> Hence, the TG analysis provides the evidences for the presence of all the components in the prepared tricomponent scaffolds.

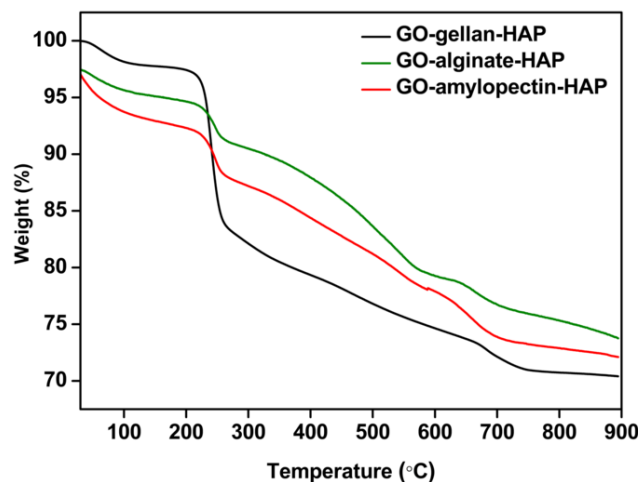


Fig. 1 TGA images of tricomponent scaffolds

### FTIR analysis

FTIR spectra of raw materials and tricomponent scaffolds were recorded to identify the interactions between the components in scaffolds and shown in Fig. 2. All characteristic peaks for HAP 3570, 1460, 1049, 966, 881 and 634  $\text{cm}^{-1}$  were observed.<sup>11,23</sup> The appearance of peaks corresponding to OH stretching at 3352  $\text{cm}^{-1}$ , C=O at 1716  $\text{cm}^{-1}$ , C=C vibration at 1620  $\text{cm}^{-1}$ , C-OH stretching at 1224  $\text{cm}^{-1}$  and C-O-C stretching at 1051  $\text{cm}^{-1}$  confirmed the oxidation product of graphite, the GO.<sup>43</sup> The characteristic bands OH stretching at 3419  $\text{cm}^{-1}$ , C-H stretching at 2121  $\text{cm}^{-1}$ , asymmetric carboxylate at 1612  $\text{cm}^{-1}$ , symmetric carboxylate at 1400  $\text{cm}^{-1}$  and pyranoside ring at 1047  $\text{cm}^{-1}$  for gellan,<sup>44,45</sup> OH stretching at 3414  $\text{cm}^{-1}$ , C-H stretching vibrations at 2924  $\text{cm}^{-1}$ , asymmetrical COO<sup>-</sup> stretching at 1612  $\text{cm}^{-1}$ , symmetrical COO<sup>-</sup> stretching at 1402  $\text{cm}^{-1}$  and C-O-C stretching (saccharide structure) at 1064  $\text{cm}^{-1}$  for alginate,<sup>46,47</sup> and OH stretching at 3445  $\text{cm}^{-1}$ , asymmetric C-H stretching at 2940  $\text{cm}^{-1}$ , adsorbed water at 1629  $\text{cm}^{-1}$ , angular deformation of C-H at 1399  $\text{cm}^{-1}$ , C-O ether stretching at 1090  $\text{cm}^{-1}$  and C-O alcohol stretching at 1028  $\text{cm}^{-1}$  for amylopectin<sup>11,48</sup> confirmed the presence of gellan, alginate and amylopectin. In the FTIR spectrum of GO-gellan-HAP, GO-alginate-HAP and GO-amylopectin-HAP scaffolds, all the characteristic peaks of the individual components were observed with a slight shift in the peak values. The mixed characteristic peaks confirmed the dispersion of HAP and GO in the polysaccharides such as alginate, amylopectin and gellan. Further, the chemical interactions in the tricomponent scaffolds were indicated by the shift in the peaks with reduced peak intensity.<sup>11,22</sup> Furthermore, the shift of phosphate peak in HAP (1049  $\text{cm}^{-1}$ ) to lower wave numbers confirmed the strong intermolecular hydrogen bonding between HAP and GO.<sup>49</sup>

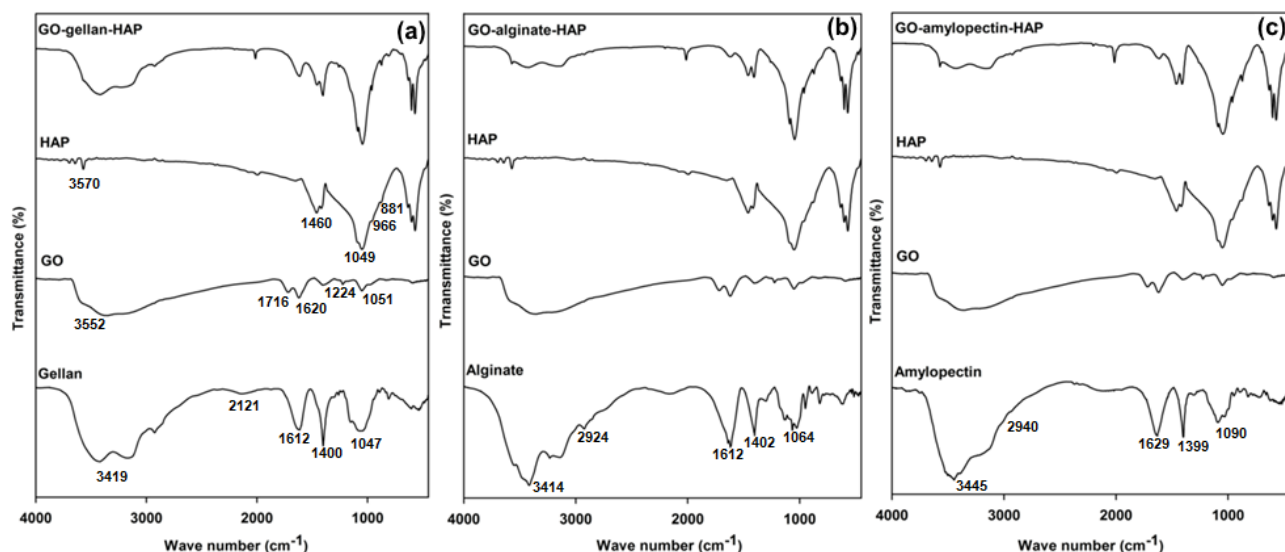


Fig. 2 FTIR spectra of (a) GO-gellan-HAP, (b) GO-alginate-HAP and (c) GO-amylopectin-HAP scaffold

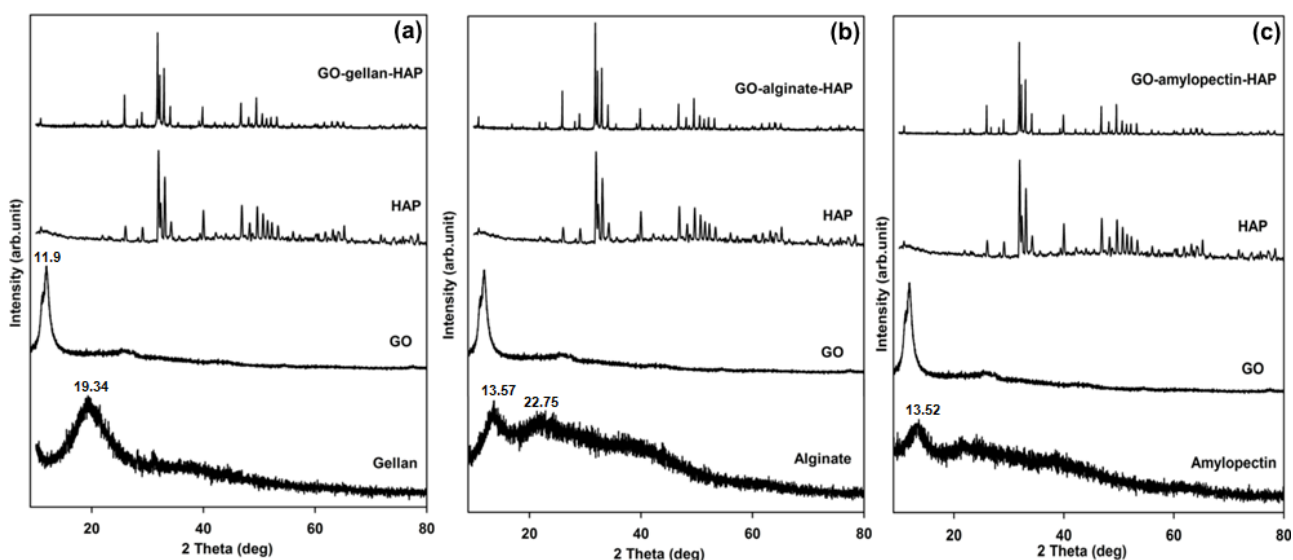


Fig. 3 XRD pattern of (a) GO-gellan-HAP, (b) GO-alginate-HAP and (c) GO-amylopectin-HAP scaffold

### XRD analysis

Phase and crystallinity of the prepared tricomponent scaffolds were identified using XRD analysis and shown in Fig 3. The diffraction pattern of isolated HAP was found to be in good conformity with the standard values of HAP (JCPDS-09-0432/1996). The disappearance of the characteristic peak of graphite at 26.4° with a d-spacing 3.37Å and the appearance of the characteristic peak of GO at 11.9° with a d-spacing 7.43Å confirmed the oxidation of graphite to GO. The higher d-spacing value of GO was due to the presence of oxygen containing functional groups such as carboxyl, hydroxyl, epoxy and other structural defects.<sup>43</sup> The broad diffraction peaks obtained for gellan (19.34°), alginate (13.57° and 22.75°) and amylopectin (13.62°) indicated the amorphous nature with lower crystallinity.<sup>7</sup> The shift of characteristic peaks of HAP, GO, gellan, alginate and amylopectin for all the composite and broadening of peaks of HAP along with peaks of reduced intensity for GO and polysaccharides in the XRD patterns of tricomponent scaffolds

for GO-gellan-HAP, GO-alginate-HAP and GO-amylopectin-HAP confirmed the formation of composites and the interactions between HAP, GO and polysaccharides.<sup>11,18,21-22</sup>

### FE-SEM analysis

Morphological studies of prepared tricomponent scaffolds were analyzed by FE-SEM analysis and shown in Fig. 4. FE-SEM images of the isolated HAP (Fig.4a) confirmed the crystalline nature with crystal size of 300-400 nm. Morphology of GO-alginate-HAP (Fig 4c) and GO-amylopectin-HAP (Fig 4c) confirmed the porous nature with pore size 56-66 μm and 89-101 μm respectively, whereas GO-gellan-HAP (Fig 4b) showed low porosity with pore size 17-32 μm (Fig 4e insert) which may be attributed to the rigidity and higher viscous nature of the gellan. The lower porosity possessed by GO-gellan-HAP scaffolds was further corroborated from the cross sectional SEM images (Fig 5a, 5b & 5c) of tricomponent scaffolds. The uniform deposition of HAP on polysaccharides can be visualized and confirmed by FE-SEM images (Fig 4b, 4c & 4d).

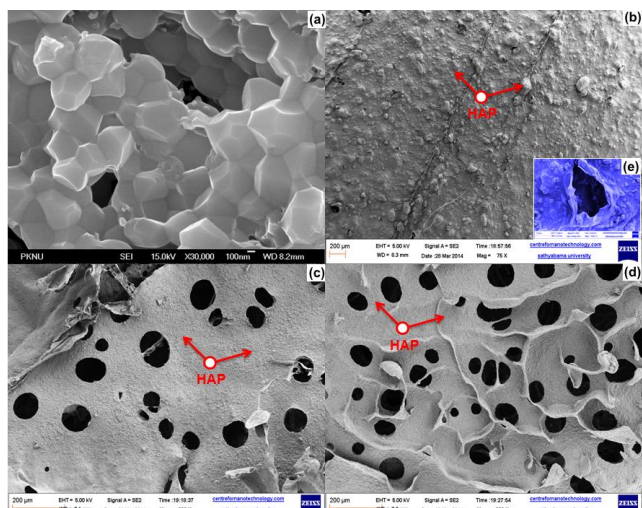


**Fig. 4** FE-SEM images of (a) HAP (b) GO-gellan-HAP (insert (e) higher magnification), (c) GO-alginate-HAP and (d) GO-amylopectin-HAP scaffold

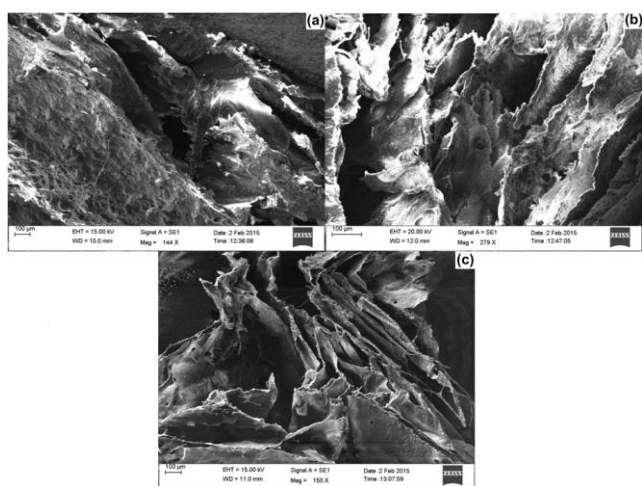


**Fig. 5** Cross sectional FE-SEM images of (a) GO-gellan-HAP, (b) GO-alginate-HAP and (c) GO-amylopectin-HAP scaffold

### Porosity analysis

Natural bone is composed of collagen-HAP composite with 10-30% porous hard outer layer and 30-90% porous interior. The higher porosity of scaffold is an important factor for new bone tissue formation which allows the migration and proliferation of osteoblasts and mesenchymal cells, as well as vascularization and delivering genes and proteins.<sup>1,11</sup> Total porosity of the prepared tricomponent scaffolds were determined by liquid displacement methods and the values were found to be 80.76% for GO-gellan-HAP scaffolds, 90.64% for GO-alginate-HAP and 94.79% for GO-amylopectin-HAP. The higher porosity of the prepared tricomponent scaffolds met the requirements of the material for bone tissue engineering.

### *In vitro* biocompatibility assay

Biocompatibility is a prerequisite for the use of tricomponent scaffolds in tissue engineering. The cell viability and proliferation of MG 63 cells on the prepared tricomponent scaffolds were evaluated using the MTT assay and shown in Fig. 6. When seeding 3D scaffold with cells it is desired that the cells will

infiltrate and colonize the scaffold laying down their own ECM. The higher porosity (~90%)<sup>50</sup> and its ability to promote the cell migration and tissue growth are some of the advantages of the scaffolds prepared.<sup>51</sup> The cell proliferation increased with increasing days as shown in table 1 which proves their biocompatibility. The results revealed that the prepared tricomponent scaffolds does not exert any cytotoxic effect on MG 63 cell line. Recent studies proved that the cytocompatibility of GO was due to the presence of oxygen containing functionalities.

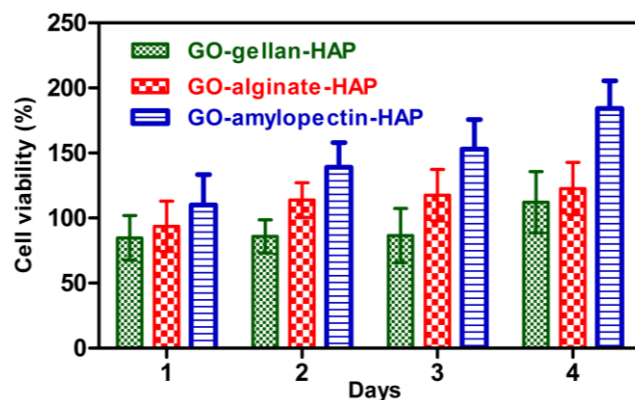


**Fig. 6** *In vitro* cytotoxicity assay of GO-gellan-HAP, GO-alginate-HAP and GO-amylopectin-HAP scaffolds on MG 63 cell line as a function of days. Values are expressed as mean  $\pm$  standard deviation ( $P < 0.0001$ ,  $n = 3$ )

**Table 1** Cell viability of tricomponent composite scaffolds

Scaffold	Cell viability (%)			
	1 <sup>st</sup> day	2 <sup>nd</sup> day	3 <sup>rd</sup> day	4 <sup>th</sup> day
GO-gellan-HAP	84.73	85.97	86.60	112.18
GO-alginate-HAP	93.55	113.89	117.55	122.67
GO-amylopectin-HAP	110.11	139.00	153.11	184.22

GO and polysaccharides are polar with negatively charged functionalities including hydroxyl and carboxyl groups. The presence of a polar constituent plays a prominent role in the biological functions of cells as they enhance the interaction with the constituent of cells and culture medium. In this case, osteoconductive HAP along with negatively charged GO and polysaccharides (gellan, alginate and amylopectin) enhance the cell matrix interactions through their negatively charged species. Hence, these materials can be used in human body as scaffolds or implants. Among the tricomponent scaffolds, GO-amylopectin-HAP exhibited higher cell proliferation due to higher porosity.<sup>21,30,52</sup> This suggest that the pores of the scaffold mainly influence the cell adhesion and proliferation through infiltration of cells on the scaffolds. These results indicated that the higher cell proliferation and cell growth may be due to the influence of multiple factors including negatively charged components,

porosity, and incorporation of osteoconductive HAP.

### Alkaline phosphatase activity

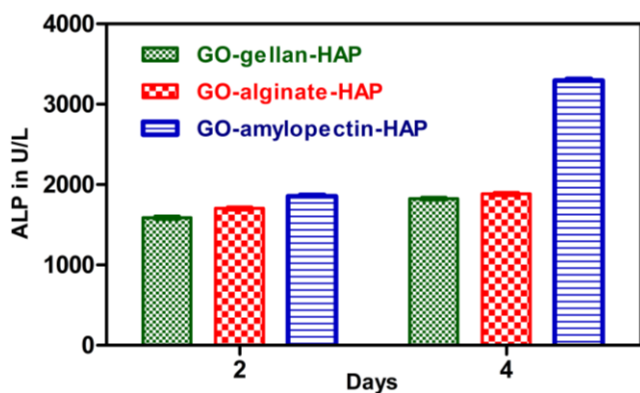


**Fig. 7** ALP assay of GO-gellan-HAP, GO-alginate-HAP and GO-amylopectin-HAP scaffolds on MG 63 cell line. Values are expressed as mean  $\pm$  standard deviation ( $P < 0.0001$ ,  $n = 3$ )

Tissue engineering is an emerging area, wherein the success of osteogenesis is measured by robust ALP expression which inevitably leads to mineralization of the neotissue. Human have four ALP genes corresponding to intestinal, placental, placental-like and liver/bone/kidney. According to booster hypothesis, the function of ALP is to increase the concentration of inorganic phosphate.<sup>53</sup> Differentiation of cells is an important process for bone regeneration. It was reported that the GO included HAP composites showed significantly higher ALP activity. This is a positive indication for the inclusion of GO in the scaffolds for better cell differentiation.<sup>18,27</sup> In our *in vitro* test, the differentiation of MG 63 cells onto scaffolds were determined using ALP activity. ALP activity was used as a biochemical marker for the determination of osteoblast phenotype and was considered as an important factor in determining bone differentiation and mineralization.<sup>54-57</sup> ALP activity of prepared tricomponent scaffolds are shown in Fig. 7. ALP on the scaffolds increased with increasing days, which is the positive indication for the mineralization for producing inorganic phosphate ion. Among the scaffolds, GO-amylopectin-HAP exhibited higher ALP activity and this is good correlation with the cytotoxicity assay also.

### Cell attachment assay using stains

Cell attachment on tricomponent scaffolds was studied using Hoechst and acridine orange stain and the images are shown in Fig. 7. The fluorescent Hoechst 33342 DNA can be used to detect the adherence of cells to visualize nuclei and mitochondria.<sup>11,58</sup> Whereas, acridine orange can bind with double stranded nucleic acid (DNA) and emits green fluorescence or red fluorescence if bound to single stranded nucleic acid (RNA). Viable cells have uniform bright green nuclei with an organized structure.<sup>59</sup> The cell attachment assay on a tricomponent scaffolds of Hoechst stain images (Fig 7 a, b & c) (blue fluorescence) and acridine orange stain images (Fig 7 d, e & f) (green fluorescence) demonstrated that the MG 63 cell line was metabolically active. The uniform green fluorescence images observed in the Fig 7 d, e & f confirmed the presence of viable cells which may be due to the interaction of DNA in the viable cells with acridine orange dye. Most cells on the scaffolds were well distributed and

exhibited highly branched morphology after 4 days. The hydroxyl groups present in GO and polysaccharides provide the sites to facilitate cell adhesion by retaining and recruiting cells on to the scaffold surface. Further, hydrophilic GO improves the interfacial adhesion with cell membrane.

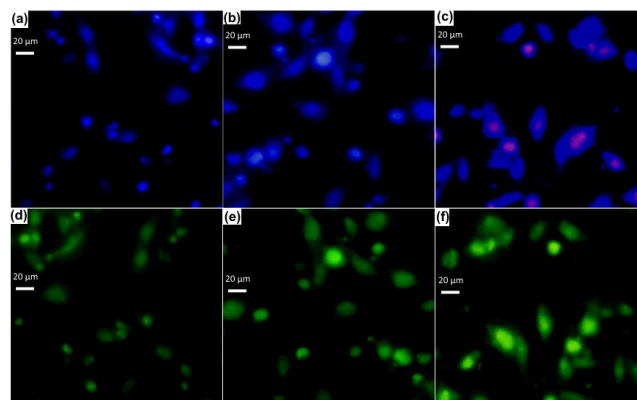


**Fig. 8** Optical microscopy images of Hoechst 33342 stained cells grown on (a) GO-gellan-HAP, (b) GO-alginate-HAP and (c) GO-amylopectin-HAP scaffolds and acridine orange stained cells grown on (d) GO-gellan-HAP, (e) GO-alginate-HAP and (f) GO-amylopectin-HAP scaffolds

From the previous report, it has been concluded that GO provided a platform to construct a biointerface with the dimensional capability for the growth of cells.<sup>52</sup> The adhered cells on GO-alginate-HAP and GO-amylopectin-HAP scaffolds were higher when compared to GO-gellan-HAP, due to the porosity differences. This behaviour can be well correlated with the MTT assay. These results provide the evidences for the adhesion of cells on to the tricomponent scaffolds.<sup>45</sup>

### Compressive strength

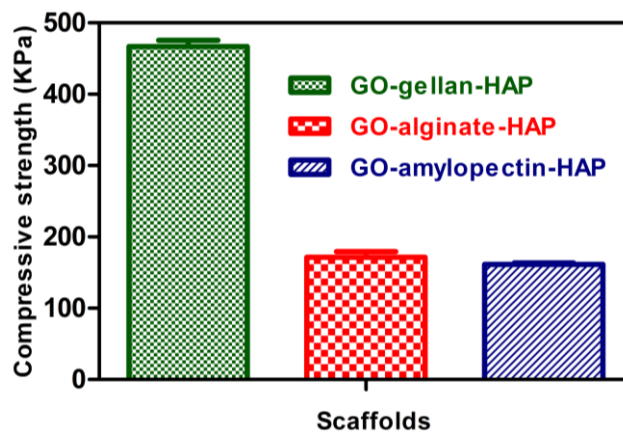


**Fig. 9.** Compressive strength images of tricomponent scaffolds. Values are expressed as mean  $\pm$  standard deviation

Scaffold materials used for bone tissue engineering should undergo various amounts of stresses during new bone formation for the protection of cultured cells from damaging and to keep the integrity of the scaffold.<sup>60</sup> The roughness of HAP and GO would contribute to mechanical interlocking with the macromolecular chains of polysaccharides. Compressive strength of the freeze dried tricomponent scaffolds was determined and shown in Fig. 9. All scaffold materials exhibited sponge like behaviour. The compressive strength value determined was  $466.8 \pm 19$  for GO-

gellan-HAP,  $171 \pm 17$  for GO-alginate-HAP and  $161 \pm 4$  for GO-amylopectin-HAP scaffolds. The decrease in compressive strength is mainly due to the increasing porosity and pore size of the scaffolds along with decreasing viscosity of polysaccharide. Moreover, increasing porosity will act as a barrier against crack propagation due to the uniform distributing of applied stress in the porous.<sup>52,61</sup>

## Experimental

### Materials

HAP was isolated from the chicken bones (purchased from local slaughterhouse) by the thermal calcinations method. The MG 63 cell line was obtained from the National Center for Cell Science, Pune, India. Graphite, amylopectin, sodium alginate, gellan gum, 3-(4,5-dimethylthiazol-2-yl)-2,5-diphenyltetrazolium bromide (MTT), acridine orange and Bisbenzimidazole Hoechst 33342 stains were purchased from Sigma Aldrich. Dulbecco's Modified Eagle's Medium (DMEM) was purchased from HIMEDIA. Sodium phosphate buffer, NaCl and KCl were purchased from Merck. NaOH, KMnO<sub>4</sub>, NaNO<sub>3</sub>, 30% H<sub>2</sub>O<sub>2</sub>, con.H<sub>2</sub>SO<sub>4</sub> (AR grade) were purchased from the S.D. fine chemicals.

### Isolation of HAP from chicken bone

HAP was isolated by thermal calcinations method as reported previously by our group.<sup>38</sup> The chicken bones were washed with concentrated NaOH solution followed by rinsing with water to remove the traces of meat, skin and other impurities present on the surface of the bones. Then the bones were dried in hot air oven at 100 °C and grained in to small pieces. Pre treated chicken bones were subjected to thermal calcinations at 800 °C with 20 h holding time in an electrical muffle furnace (SUNSIM, India).

### Preparation of graphene oxide

GO was prepared from graphite by modified Hummer's method as reported by Marcano et al.<sup>62</sup> Con. H<sub>2</sub>SO<sub>4</sub> (23 ml) was added to a mixture of graphite (1 g) flakes and NaNO<sub>3</sub> (0.5 g), then the mixture was cooled to 0 °C using an ice bath. KMnO<sub>4</sub> (3 g) was added slowly in portions to maintain the reaction temperature below 20 °C. The reaction was warmed to 35 °C and stirred for 7 h. Additional KMnO<sub>4</sub> (3 g) was added in one portion, and the reaction was stirred for 12 h at 35 °C. The reaction mixture was cooled to room temperature and poured onto the ice (~400 ml) with 30% H<sub>2</sub>O<sub>2</sub> (3 ml). The suspension was filtered and successively washed with 30% HCl, double distilled water and ethanol. The obtained solid product was oven dried.

### Preparation of GO-polysaccharide-HAP scaffold

1.74 g of polysaccharides (gellan gum or alginate or amylopectin) was dissolved in 100 ml of double distilled water. 60 mg of GO was dispersed in distilled water by sonication and added drop wise to the polysaccharide solution then stirred for 3 h. 4.2 g of isolated HAP was suspended in 50 ml of distilled water and added slowly to the GO-polysaccharide solution and stirred for 24 h. The resultant composite solution mixture was transferred into 12 well plates with 2 g solution per well. The samples were freeze dried at -80 °C and lyophilized with a freeze dryer to form scaffold.

### General characterization

The thermal stability of the composite scaffold was studied using thermo gravimetric (TG) (SDTQ 600 TA Instrument, USA) with scan range of 50 °C to 900 °C at a constant heating rate of 10 °C/min in the nitrogen atmosphere. The vibrational frequency of the samples was studied by Fourier transformed infrared spectroscopy (FTIR) (Jasco FTIR4100, Japan) and the spectrum was recorded within the range of 4000 cm<sup>-1</sup> to 500 cm<sup>-1</sup> using KBr. The phase and crystallinity of the samples were examined by powder X-ray diffraction (XRD) (Bruker, D8 Advance X-ray Diffraction spectrophotometer, German) at room temperature using CuKα as the radiation source with the wavelength 1.504 Å, over the angle range 10° to 80°, step size 0.02° and scan speed 0.5°/min. The resultant XRD profile of the isolated HAP was compared with the standard Joint Committee on Powder Diffraction Standards (JCPDS) cards available in the system software. Further, the morphology of the tricomponent scaffolds was studied by field emission scanning electron microscopy (FE-SEM) (SUPRA 55, Carl Zeiss, Germany) analysis.

### Porosity measurements

Porosity is an important property for the cell proliferation. The total porosity of the scaffold was obtained by the liquid displacement method.<sup>11</sup> Initially, the volume of dry ethanol and dry weight of the scaffold was measured. Then the scaffold was immersed in dry ethanol for 48 h. After 48 h, a scaffold was taken out from ethanol and the weight of the scaffold was measured. The total porosity was calculated using the equation

$$\text{Porosity} = (W_1 - W_3) / (W_2 - W_3)$$

Where W<sub>1</sub> = initial weight of the scaffold, W<sub>2</sub> = sum of weights of ethanol and submerged scaffold, W<sub>3</sub> = weight of ethanol after the removal of scaffold.

### In vitro cell proliferation assay of scaffolds

The MG-63 cells were plated separately in 96 well plates at a concentration of  $1 \times 10^5$  cells/well. After 24 h, cells were washed twice with 100 μl of serum-free medium and starved for an hour at 37 °C. After starvation, cells were seeded with the scaffold material which was previously sterilized with 75% alcohol followed by 100% alcohol. Cells treated without scaffold material was used as a control. At the end of the treatment period of 1, 2, 3 and 4 days, the medium was aspirated and serum free medium containing MTT (0.5 mg/ml) was added and incubated for 4 h at 37 °C in a CO<sub>2</sub> incubator. The determinations were performed using triplicates each time.

The MTT containing medium was then discarded and the cells were washed with phosphate buffer solution (PBS) (200 μl). The formed formazan crystals were then dissolved by adding 100 μl of DMSO and this was mixed properly by pipetting up and down. Spectrophotometrical absorbance of the purple blue formazan dye was measured in a microplate reader at 570 nm (Biorad 680).<sup>11,63</sup> Cytotoxicity was determined using Graph pad prism 5 software.

### Alkaline phosphatase assay

For the determination of ALP activity, cells were cultured as per the cytotoxicity analysis, after the incubation with scaffolds for 2 and 4 days, the cells were treated with 10 μL (100 mmol/lit) of p-nitrophenyl phosphate and incubated for 30 min at 37 °C in a CO<sub>2</sub>

incubator. ALP can hydrolyze the p-nitrophenyl phosphate in to p-nitrophenol and inorganic phosphate.<sup>64</sup> The released p-nitrophenol absorbance was measured at 405 nm spectrophotometrically. The determinations were performed using triplicates each time.

#### Hoechst stain assay for cell attachment

Hoechst 33342 DNA staining has been used to identify the cell attachment and growth on scaffold material.<sup>11</sup> For this, ethanol sterilized scaffold material was placed in the cell culture plate and seeded with MG 63 cells and incubated. After 4 days of culture, media was removed from the wells and washed with PBS solution. The cells were stained with 0.5 ml of Hoechst 33342 solutions (3.5 µg/ml in PBS) and incubated for 30 min at 37 °C. After 30 min, the Hoechst stained cells were visualized and photographed under the Microscope- Olympus- version-6.0, Carl Zeiss lens, Germany.

#### Acridine orange stain assay for cell attachment

Acridine orange is used to identify both viable and apoptotic cells on scaffold materials.<sup>59</sup> For this, ethanol sterilized scaffold material was placed in the cell culture plate and seeded with MG 63 cells and incubated. After 4 days of culture, media was removed from the wells and washed with PBS solution. The cells were stained with 200 µL of dye mixture (100 µL/mg acridine orange distilled water). The suspension was immediately examined and viewed under Microscope- Olympus- version-6.0, Carl zeiss lens, Germany.

#### Compressive strength

The compressive strength of freeze dried scaffolds was obtained using universal testing machine (UTM). The tests were performed using an H5KS system (Tinius Olsen, Salfords, UK). A 5000 N load cell with the standard grips of crosshead speed of 0.5 mm min<sup>-1</sup> was used for the compression measurements. The determinations were performed using five replicates.

#### 2.12 Statistical analysis

Statistical analysis for MTT, ALP assay and compressive strength were performed using Graph pad prism 6 software and the results are presented as mean ± standard deviation.

#### Conclusion

In this study, new 3D tricomponent composite scaffolds of GO-gellan-HAP, GO-alginate-HAP and GO-amylopectin-HAP were successfully developed to mimic the role of natural bone and tested for their cytotoxicity for biocompatibility, ALP activity for cell differentiation and mineralization, cell attachment and compressive strength for biomaterials applications. The *in vitro* studies exhibited the osteoconductivity and biocompatibility of all the scaffolds. The prepared tricomponent scaffolds exhibited comparable compressive strength as reported earlier. The higher cell proliferation and biocompatibility observed in GO-amylopectin-HAP can be attributed to higher pore size and porosity.

#### Acknowledgements

The authors gratefully acknowledge the management of the VIT

University, Vellore, India for the facilities offered to carry out this piece of work. One of the authors R. Rajesh gratefully acknowledges the RA fellowship from VIT University. The authors also acknowledge the powder XRD facility at SAS, VIT University, jointly funded by VIT and FIIST, DST India. Further, the authors thank the Pondicherry Center for Biological Sciences (PCBS), Pondicherry for the *in vitro* studies.

#### References

- 1 S. Bose and M. Roy, *Trends in Biotechnology*, 2012, **30**, 546.
- 2 J. Malda and C.G. Fronzoza, *Trends in Biotechnology*, 2006, **24**, 299.
- 3 M.E. Gomes and R.L. Reis, *International Materials Review*, 2004, **49**, 261.
- 4 J.F. Mano, G.A. Silva, H.S. Azevedo, P.B. Malafaya, R.A. Sousa, S.S. Silva, L.F. Boesel, J.M. Oliveira, T.C. Santos, A.P. Marques, N.M. Neves and R.L. Reis, *Journal of the Royal Society Interface*, 2007, **4**, 999.
- 5 F.M.P. Tonelli, A.K. Santos, K.N. Gomes, E. Lorencon, S. Guatimosim, L.O. Ladeira and R.R. Resende, *International Journal of Nanomedicine*, 2012, **7**, 45111.
- 6 K.W.-H. Lo, B.D. Ulery, K.M. Ashe, C.T. Laurencin, *Advanced Drug Delivery Reviews*, 2012, **64**, 1277.
- 7 K.Y. Lee, D.J. Mooney, *Progress in Polymer Science*, 2012, **37**, 106.
- 8 M.V. Jose, V. Thomas, K.T. Johnson, D.R. Dean, E. Nyairo, *Acta Biomaterialia* 2009, **5**, 305.
- 9 F.P.W. Melchels, M.A.N. Domingos, T.J. Klein, J. Malda, P.J. Bartolo, *Progress in Polymer Science*, 2012, **37**, 1079.
- 10 A.L. Rossi, I.C. Barreto, W.Q. Maciel, F.P. Rosa, M.H. Rocha-Leao, J. Werckmann, A.M. Rossi, R. Borojevic, M. Farina, *Bone*, 2012, **50**, 301.
- 11 J. Venkatesan, R. Pallela, I. Bhatnagar and S.-K. Kim, *International Journal of Biological Macromolecules*, 2012, **51**, 1033.
- 12 J.T. Oliveira, T.C. Santos, L. Martins, L. Picciochi, A.P. Marques, A.G. Castro, N.M. Neves, J.F. Mano and R.L. Reis, *Tissue Engineering Part A*, 2010, **16**, 343.
- 13 A.R. Shrivats, M.C. McDermott and J.O. Hollinger, *Drug Discovery Today*, 2014, **19**, 781.
- 14 D. Dyondi, T.J. Webster and R. Banerjee, *International Journal of Nanomedicine*, 2013, **8**, 47.
- 15 G. Muzio, G. Martinasso, F. Baines, R. Frairia, C. Vitale-Brovarone, R.A. Canuto, *Journal of Biomaterials Applications*, 2014, **29**, 728.
- 16 R. Kane, P.X. Ma, *Materials Today*, 2013, **16**, 418.
- 17 M. Descamps, J.C. Hornez and A. Leriche, *Journal of the European Ceramic Society*, 2009, **29**, 369.
- 18 F. Mohandes and M. Salavati-Niasari, *RSC Advances*, 2014, **4**, 25993.
- 19 P.T.S. Kumar, S. Srinivasan, V.K. Lakshmanan, H. Tamura, S.V. Nair and R. Jayakumar, *Carbohydrate Polymers*, 2011, **85**, 584.
- 20 R. Rajesh, N. Senthilkumar, A. Hariharasubramanian and Y.D. Ravichandran, *International Journal of Pharmacy and Pharmaceutical Sciences*, 2012, **4**, 23.
- 21 J. Venkatesan, Z.-J. Qian, B. Ryu, N.A. Kumar and S.-K. Kim, *Carbohydrate Polymers*, 2011, **3**, 569.
- 22 R. Rajesh, A. Hariharasubramanian, N. Senthilkumar and Y.D. Ravichandran, *International Journal of Pharmacy and Pharmaceutical Sciences*, 2012, **4**, 716.
- 23 R. Rajesh, A. Hariharasubramanian and Y.D. Ravichandran, *Phosphorus, Sulfur, and Silicon and the Related Elements*, 2012, **187**, 914.
- 24 T. Kuilla, S. Bhadra, D. Yao, N.H. Kim, S. Bose and J.H. Lee, *Progress in Polymer Science*, 2010, **35**, 1350-1375.
- 25 I. Armentano, M. Dottori, E. Fortunati, S. Mattioli and J.M. Kenny, *Polymer Degradation and Stability*, 2010, **95**, 2126.

- 26 Y. Pan, T. Wu, H. Bao and L. Lin, *Carbohydrate Polymers*, 2011, **83**, 1908.
- 27 M. Li, Q. Liu, Z. Jia, X. Xu, Y. Cheng, Y. Zheng, T. Xi and S. Wei, *Carbon*, 2014, **67**, 185.
- 5 28 T. Ma, P.R. Chang, P. Zheng, X. Ma, *Carbohydrate polymers*, 75 2013, **94**, 63-70.
- 29 S. Kang, J.B. Park, T.-J. lee, S. Ryu, S.K. Bang, W.-G. La, M.-K. Noh, B.H. Hong, B.-S. Kim, *Carbon*, 2015, **83**, 162.
- 10 30 Y. Li, C. Liu, H. Zhai, C. Zhu, H. Pan, X. Xu and R. Tang, *RSC Advances*, 2014, **4**, 25398.
- 31 P. Gentile, M. Mattioli-Belmonte, V. Chiono, C. Ferretti, F. Baino, C. Tonda-Turo, C. Vitale-Brovarone, I. Pashkuleva, R.L. Reis, G. Ciardelli, *Journal of Biomedical Materials research A*, 2012, **100**, 2654.
- 15 32 W. Lu, K. Ji, J. Kirkham, Y. Yan, A.R. Boccaccini, M. Kellett, 85 Y. Jin and X.B. Yang, *Cell Tissue Research*, 2014, **356**, 97.
- 33 F.J. O'Brein, *Materials Today*, 2011, **14**, 88.
- 34 L. Meinel, V. Karageorgiou, R. Fajardo, B. Snyder, V. Shinde-Patil, L. Zichner, D. Kalpan, R. Langer, G. Vunjak-Novakovic, *Annals of Biomedical Engineering*, 2004, **32**, 112.
- 20 35 A. Jonitz, J. Wieding, K. Lochner, M. Cornelsen, H. Seitz, D. Hansmann, R. Bader, *Materials*, 2011, **4**, 1249-1259.
- 36 N.G. Rim, C.S. Shin, H. Shin, *Biomedical Materials*, 2013, **8**, 014102 (14pp).
- 25 37 F. Tamimi, J. Torres, K. Al-Abedalla, E. Lopez-Cabarcos, M.H. Alkhraisat, D.C. Bassett, U. Gbureck, J.E. Barralet, *Biomaterials*, 2014, **35**, 5346.
- 38 I.-K. Yoon, J.-Y. Hwang, J.-W. Seo, W.-C. Jang, H.-W. Kim and U.S. Shin, *Carbon*, 2014, **77**, 379.
- 30 39 M. Li, Q. Liu, Z. Jia, X. Xu, Y. Shi, Y. Cheng, Y. Zheng, T. Xi and S. Wei, *Applied Surface Sciences*, 2013, **284**, 804.
- 40 N. Barbani, M.L. Coluccio, C. Cristallini, G.D. Guerra and E. Rosellini, *Journal of Applied Polymer Science*, 2010, **118**, 3131.
- 35 41 M. Ionita, M.A. Pandeale and H. Iovu, *Carbohydrate Polymers*, 2013, **94**, 339.
- 42 R. Rajesh, Y.D. Ravichandran, N.A.N. Raj and N. Senthilkumar, *Polymer-Plastics Technology and Engineering*, 2014, **53**, 1105.
- 40 43 G.M. Neelgund, A. Oki and Z. Luo, *Materials Research Bulletin*, 2013, **48**, 175.
- 44 J. Roman, M.V. Cabanas, J. Pena and M.V.-Regi, *Science and Technology of Advanced Materials*, 2001, **12**, 045003 (9pp).
- 45 45 G. Ciardelli, V. Chiono, G. Vozzi, M. Pracella, A. Ahluwalia, N. Barbani, C. Cristallini and P. Giusti, *Biomacromolecules*, 2005, **6**, 1961.
- 46 L. Wang, Y. Li and C. Li, *Journal of Nanoparticle Research*, 2009, **11**, 691.
- 47 D. Leal, B. Matsuhiro, M. Rossi and F. Caruso, *Carbohydrate Research*, 2008, **343**, 308.
- 50 48 D.C. Dragunski and A. Pawlicka, *Materials Research*, 2001, **4**, 77.
- 49 M. Li, Y. Wang, Q. Liu, Q. Li, Y. Cheng, Y. Zheng, T. Xi, S. Wei, *Journal of Materials Chemistry B*, 2013, **1**, 475.
- 55 50 J.F. O'Brien, B.A. Harley, M.A. Waller, I.V. Yannas, L.J. Gibson and P.J. Prendergast, *Technology and health Care*, 2007, **15**, 3.
- 51 I.V. Yannas, E. Lee, D.P. Orgill, E.M. Skrabut and G.F. Murphy, *Proceeding of the National Academy of Sciences of the United States of America*, 1989, **86**, 933.
- 60 52 D. Depan, B. Girase, J.S. Shah, R.D.K. Misra, *Acta Biomaterialia*, 2011, **7**, 3432.
- 53 E.E. Golub and K.B.-Battaglia, *Current Opinion in Orthopaedics*, 2007, **18**, 444.
- 65 54 H. Wang, Y. Li, Y. Zuo, J. Li, S. Ma and L. Cheng, *Biomaterials*, 2007, **28**, 3338.
- 55 R. Marom, I. Shur, R. Solomon and D. Benayahu, *Journal of Cellular Physiology*, 2005, **202**, 41.
- 56 U. Stucki, J. Schmid, C.F. Hammerle and N.P. Lang, *Clinical Oral Implant Research*, 2001, **12**, 121.
- 57 L. Pan, X. Pei, R. He, Q. Wan and J. Wang, *Colloids and Surfaces B: Biointerfaces*, 2012, **93**, 226-234.
- 58 A. Stander, S. Marais, V. Stivaktas, C. Vorster, C. Albrecht, M.L. Lottering and A.M. Joubert, *Journal of Ethnopharmacology*, 2009, **124**, 45.
- 59 D. Baskic, S. Popovic, P. Ristic and N.N. Arsenijevic, *Cell Biology International*, 2006, **30**, 924.
- 60 X.Wu, Y. Liu, P. Wen, Y. Zhang, Y. Long, X. Wang, Y. Guo, F. Xing and J. Gao, *Acta Biomaterialia*, 2010, **6**, 1167.
- 80 61 U.-J. Kim, J. Park, H.J. Kim, M. Wada, D.L. Kaplan, *Biomaterials*, 2005, **26**, 2775.
- 62 D.C. Marcano, D.V. Kosynkin, J.M. Berlin, A. Sinitskii, Z. Sun, A. Slesarev, L.B. Alemany, W. Lu and J.M. Tour, *Acs Nano*, 2010, **4**, 4806.
- 63 N. Ramalingam, T.S. Natarajan, S. Rajiv, *Journal of Biomedical Materials Research Part A*, 2015, **103**, 16.
- 64 J. Venkatesan and S.-K. Kim, *Journal of Biomedical Nanotechnology*, 2012, **8**, 676.